CMOS lock-in optical sensor for parallel detection in pump-probe systems

Roger A. Light*[a], Richard J. Smith[b], Nicholas S. Johnston[a], Michael G. Somekh[a] and Mark C. Pitter[a]

[a]IBIOS, University of Nottingham, University Park, Nottingham, NG7 2RD, UK;
[b]Applied Optics, University of Nottingham, University Park, Nottingham, NG7 2RD, UK

ABSTRACT

In pump-probe type experiments the signal of interest is often a very small fraction of the overall light intensity reaching the detector. This is beyond the capabilities of conventional cameras due to the necessarily high light intensity at the detector and its limited dynamic range. To overcome these problems, phase-sensitive or lock-in detection with a single photodiode is generally used. In phase-sensitive detection, the pump beam is modulated and the probe beam is captured with a photodiode connected to a lock-in amplifier running from the same reference. This provides very narrowband detection and moves the signal away from low frequency noise. We have developed a linear array detector that can perform shot-noise limited lock-in detection in 256 parallel channels. Each pixel has four independent wells to allow phase-sensitive detection. The depth of each well is massively increased and can be controlled on a per-pixel basis allowing the gain of the sensor to be matched to the incident light intensity, improving noise performance. The array reduces the number of dimensions that need to be sequentially scanned and so greatly speeds up acquisition. Results demonstrating spectral parallelism in pump-probe experiments are presented where the a.c. amplitude to background ratio approaches 1 part in one million.

Keywords: CMOS image sensor, active pixel sensor, modulated light, phase sensitive detection

1. INTRODUCTION

Scientific imaging often poses a set of problems that are not well catered for by conventional commercial cameras. Two main problem areas exist: where the overall light level is very low and where there is a high light level at the detector, but only a small proportion of this is the signal of interest. Conventional cameras are designed for imaging the every day world, where contrast is relatively high and the dynamic range requirements of the camera are modest. In most cases the noise performance of the device is much less important than the size and number of pixels.

In low light experiments even the brightest of signals is small so great care must be taken to reduce noise. The dominant noise sources here are dark current and read noise. In astronomy, detectors are typically cryogenically cooled to reduce the dark current to a minimum, and are read out very slowly to reduce the read noise[1,2]. Another example of this type of imaging is found in fluorescence microscopy in the biology field, where the signal of interest is produced with fluorescent markers placed selectively in a sample. The fluorescence caused by the markers is very dim. Conventional cameras are not suited to this type of work, but there are alternatives such as the electron multiplying CCD which is popular because of its superior low light performance.

We are concerned with experiments with high light levels where the signal of interest is a small proportion of the background. To make these kinds of measurements, a high dynamic range is required. There is a lot of interest in making high dynamic range cameras using techniques such as taking multiple exposures[3,4], using multiple integration wells per pixel for low and high light conditions[5], using pixels with logarithmic response[6] or with combined linear and logarithmic response[7]. Although these cameras tend to offer impressive dynamic range results, the design intent of the pixels is to cope with a large range of light intensities in a single frame. They aren't intended to cope with small changes in intensity across the whole of their working range and as such their optimizations aren't useful here.

This problem of very low contrast is common in pump-probe type experiments[8] and is traditionally solved by using a single photodetector connected to a lock-in amplifier. The optical input to the experiment is modulated by some means

*roger.light@nottingham.ac.uk; phone 44 115 8468848; fax 44 115 9515616; nottingham.ac.uk/ibios

and the lock-in uses the modulation clock as a reference input. This setup has a number of advantages. The modulation the signal of interest in the frequency domain and moves it away from low frequency noise sources. The single photodetector can be of very high quality and it operates in continuous time mode so is very light efficient. The lock-in amplifier acts as a high quality band pass filter so removes further noise. The major disadvantage is that there is only a single detector, so the sample must be mechanically scanned to build up an image. Using multiple detectors and lock-ins becomes rapidly impractical.

In order to reduce the amount of time taken for an experiment by moving to a multiple detector solution, lock-in functionality must be implemented at each pixel of the detector. This type of camera, capable of operating as a lock-in detector, is known as a modulated light camera. A number of approaches have been proposed to do this[9-14], but the simplest is known as phase stepping.

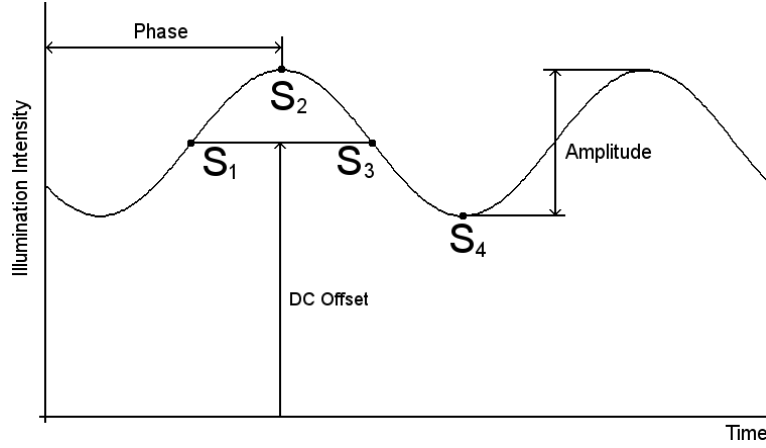
Figure 1. Modulated photocurrent at detector with signal parameters ad sample points

The signal shown in Fig. 1 represents the modulated photocurrent at the detector. The signal has three unknown parameters: the d.c. offset (B), the a.c. amplitude (A) and the phase (ϕ). We know the frequency because we are producing the modulation. Four samples of the waveform, S_1 to S_4, are taken at $90°$ to one another as follows:

$$S_1 = B + A\sin(\phi + 0) = B + A\sin(\phi) \tag{1}$$

$$S_2 = B + A\sin(\phi + 90) = B + A\cos(\phi) \tag{2}$$

$$S_3 = B + A\sin(\phi + 180) = B - A\sin(\phi) \tag{3}$$

$$S_4 = B + A\sin(\phi + 270) = B - A\cos(\phi) \tag{4}$$

Equations 1-4 can be used to calculate the d.c., amplitude and phase as follows:

$$B = \frac{S_1 + S_2 + S_3 + S_4}{4} \tag{5}$$

$$A = \frac{\sqrt{(S_1 - S_3)^2 + (S_2 - S_4)^2}}{2} \tag{6}$$

$$\phi = \tan^{-1}\frac{S_1 - S_3}{S_2 - S_4} \tag{7}$$

As there are only three unknowns it is possible to reduce the number of samples taken to just three, but using four gives a more robust result and the calculation required to reconstruct the parameters is much more straightforward.

Taking four samples like this allows us to produce lock-in behavior at the pixel level. Unlike the low light situation, the limiting factor on performance here is shot noise. For a measurement of N photons, the shot noise and hence signal to

noise ratio associated with the measurement is $\sqrt{N}$. This means that for a measurement where the signal of interest is 10^{-6} of the background, at least 10^{12} photons must be collected. It is therefore important to waste as few photons as possible. This is done by using an integrating pixel, the most commonly used pixel design. By using an integrating pixel the four samples are each taken for almost 90° of the modulation time period rather than the instantaneous sampling shown in Fig. 1. It is also important to increase the number of photons a single exposure can cope with (the well depth), to reduce the number of frames that are required to reach a given shot noise performance. Consumer devices tend to have a very small well depth which makes them very sensitive to light, but limits their noise performance. A device with well depth of 30 ke$^-$ has a best case signal to noise ratio of 173, or 7.4 bits, assuming that it is shot noise limited. Typical scientific cameras have a well depth of a few hundred thousand electrons.

2. CAMERA ARCHITECTURE AND OPERATION

Our sensor is a linear array of 256 pixels fabricated in the Austriamicrosystems C35B4C3 process, a 0.35 μm 2-poly 4-metal, 3.3 V standard CMOS process.

2.1 Pixel design

The pixel design is based on the standard four transistor active pixel circuit, but with four output channels per pixel to allow modulated detection. Fig. 2 shows the basic circuit diagram for the pixel, with only one output channel shown.
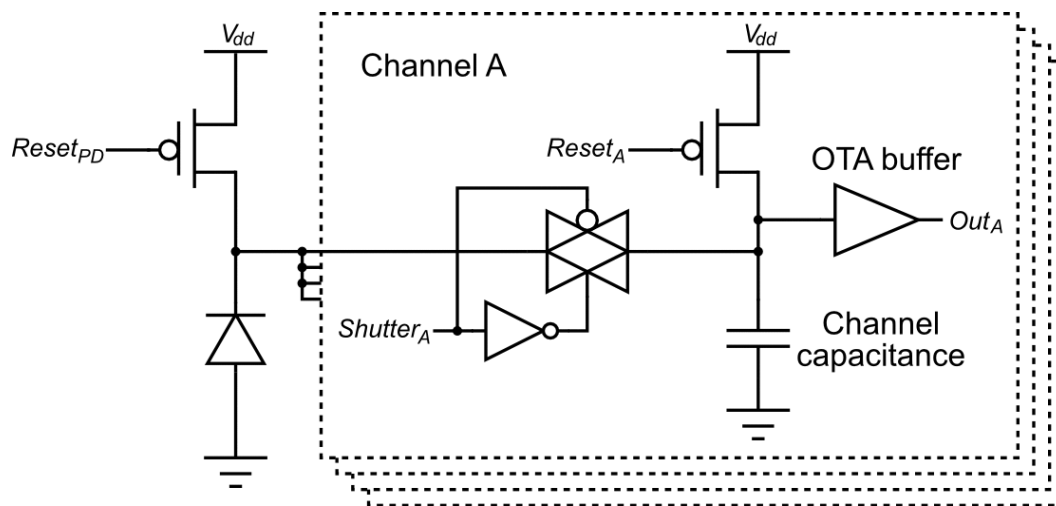

Figure 2. Basic pixel schematic

The basic operation of the pixel is as follows. To make an exposure on channel A, the Reset$_{PD}$, Reset$_A$ and Shutter$_A$ lines are pulled low and Reset$_{B-D}$ and Shutter$_{B-D}$ are held high. The voltage across the photodiode and channel capacitance charges to V$_{DD}$. The two reset lines are now taken high to open the two reset switches. The flow of photo current through the photodiode will discharge the combined capacitance of the photodiode and channel capacitor until the Shutter$_A$ line is pulled high to end the exposure after a fixed amount of time. At this point, the voltage at the output is a measure of the light intensity during the exposure. This can now be repeated for the other four channels.

The well depth of the pixel is increased dramatically over that of conventional cameras to reduce the effect of shot noise. This is done by increasing the size of the photodiode to 480x22 μm, which results in a well depth of 20.3 Me$^-$. The pixel size is 480x25 μm which results in a fill factor of 88%. Having a long pixel also helps with alignment. The well depth is further increased with the supplementary capacitance X formed from the gate capacitance of multiple NMOS transistors. Including the photodiode, this brings the total well depth per channel to approximately 600 Me$^-$. This means that a demodulated image produced from all four channels has a well depth of 2400 Me$^-$. Assuming the detector is shot noise limited, the signal to noise ratio based on filling the well completely is 49,000 or a dynamic range of 93 dB in a single image. The well depths here are calculated based on a useful pixel output range of 3.3-0.6 V.

The chip layout is shown in Fig. 3. The pixels are arranged with the supplementary channel capacitances above and below the photodiode as shown. Even using NMOS gate capacitance for the supplementary capacitances they still occupy the majority of the area of the array. This shows that the approach of drastically increasing well depth in this way is only feasible for linear arrays.

The per-channel reset transistors (at Reset$_A$ in Fig. 2) are another addition over the standard pixel design. Two needs are met with their inclusion. The first reason is a practical one. During reset it is important to have a low resistance path to V_{DD} so that the voltage across the photodiode and capacitors will settle rapidly. By having a per-channel reset switch, a V_{DD} supply wire can be placed horizontally across the sensor for each channel. This means that the supply wire can be much thicker than if current were being drawn through the photodiode reset which helps reset occur more quickly and removes the need for another vertical wire in each pixel. It also allows each channel to have a dedicated power supply pin which can be decoupled and supplied independently. The second reason is to allow more efficient operation of the sensor by allowing the channels to be placed in reset independently of one another and the photodiode. This means that the channel capacitance can already be in reset before it is due to be exposed. When the new channel is selected, all that needs to be reset is the photodiode which usually has a much smaller well depth than the supplementary capacitance and so the time needed for reset is reduced.

Each pixel channel output is buffered using an operational transconductance amplifier (OTA). This is another departure from the design of the standard pixel made possible by the extra space available to a linear array. The OTA is powered by a 5 V supply so as well as offering superior linearity compared to the more normal source follower buffer, it also can cope with an input and output range all the way up to the 3.3 V rail.
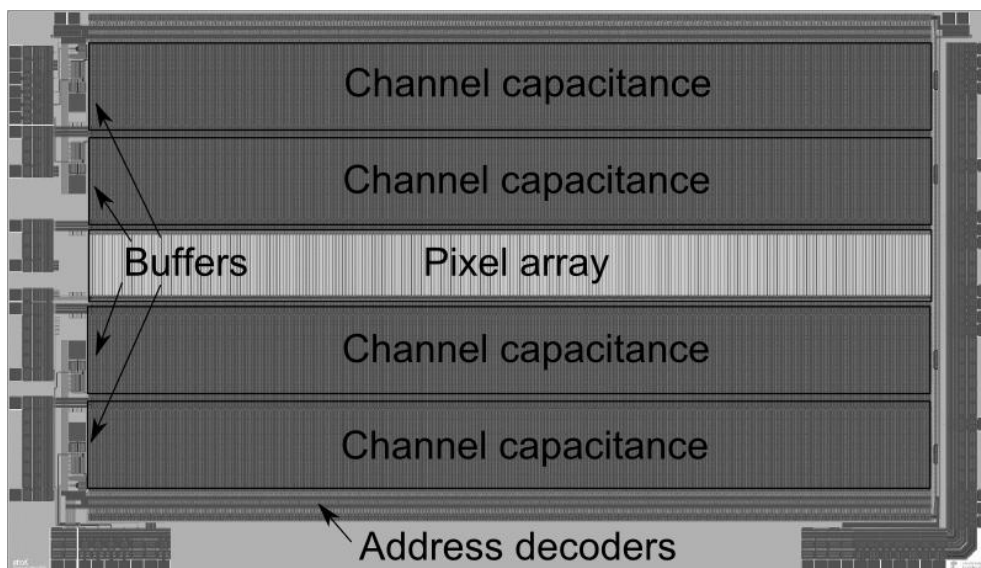

Figure 3. Chip layout.

After the pixel outputs have been multiplexed 256:1, they are sent off chip through four operational amplifier buffers, one per channel. These buffers are also powered from the 5 V rail to give improved headroom.

2.2 Per-pixel gain setting

An important feature of the sensor is the ability to program the gain of each pixel individually. This is achieved by changing the well depth of each channel by connecting and disconnecting different numbers of the supplementary capacitors to the channel. The capacitors are connected in parallel with one another through their own transmission gate as shown in Fig. X. All channels are programmed the same for each pixel. There are eleven capacitors per channel which means a total of twelve gain settings are possible. Each supplementary capacitor is 3.1 pF and the photodiode has a capacitance of approximately 1.2 pF. The per-channel well depth can be calculated with equation 8, where n is the number of supplementary capacitors that are connected.

$$W_{e^-} = 20.3 \text{Me}^- + n * 52.3 \text{Me}^-$$

(8)

The photodiode capacitance alone can be used as the well by setting $n=0$. This mode of operation gives the best sensitivity to light, but has a non-linear output due to the CV characteristics of the diode.

2.3 Acquisition system

We have designed and built a custom acquisition system for this image sensor, to allow us to place the sensor, acquisition and control electronics in a single box to give a robust and easy to use camera that is close in appearance to a commercial device. The system design is shown in Fig. 4. Control of the camera is centered on a Xilinx Spartan 3 field programmable gate array (FPGA). The FPGA connects to a computer via a USB interface which is used to send image data and receive control and configuration data. The camera uses a reference clock to generate the exposure timing. This reference clock can be generated on the FPGA and used to drive an external modulation source such as a mechanical chopper. Alternatively an external reference may be used, in which case the phase locked loop (PLL) is used to generate the 4x multiplied clock that the FPGA requires. The analog to digital converter (ADC) chip is an Analog Devices AD7625, which has a 16-bit resolution over an input range of 0-4.096 V and is operating at 1.9 Msps. The camera has two acquisition modes. If the modulation frequency is less than 1.8 kHz, then the ADC is fast enough to acquire all 256 samples of a channel in one quarter of the time of a modulation period. This means that as one channel is being exposed, a channel that was exposed in a previous step can be acquired. We call this the "streaming" mode. This arrangement means that the light is used very efficiently. The camera is always making an exposure except when the pixels are undergoing reset. This happens for 1 μs for each channel, or 4 μs per frame. At 1.8 kHz, this represents 0.72% of the frame time. At modulation frequencies greater than 1.8 kHz, the ADC is not fast enough to acquire all of the required samples within the time allowed. We use "burst" mode for frequencies greater than 1.8 kHz. In burst mode, all four exposures are taken before any acquisition takes place. Burst mode is not as light efficient as stream mode because of the separate time required for acquisition. At a modulation frequency of 1.8 kHz, burst mode spends 50% of the frame time in exposure.

It should be noted that the 1.8 kHz modulation frequency limit on stream mode is a limitation of the way the ADC is currently being used; it is not an inherent property of the camera.
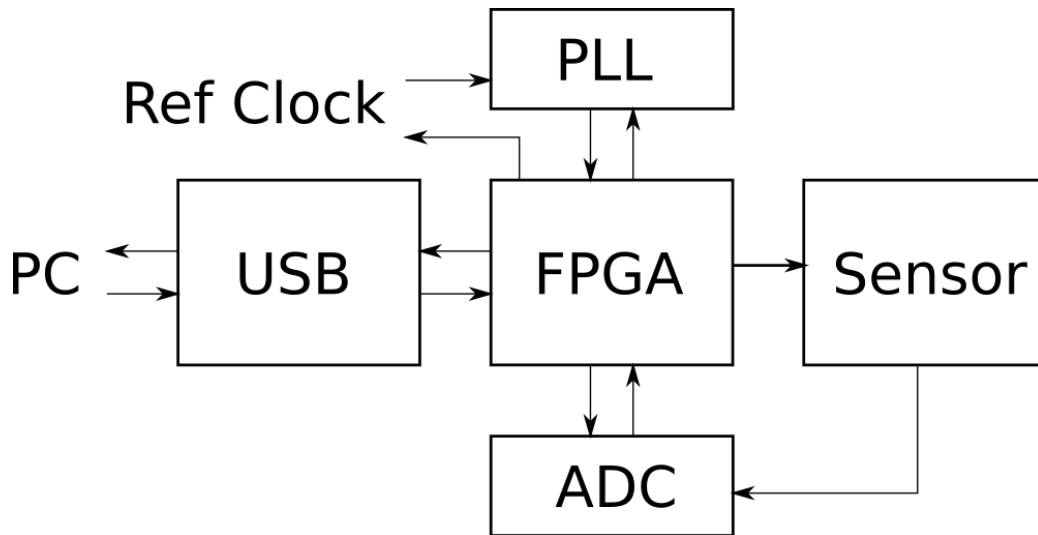

Figure 4. Camera system diagram

2.4 Theoretical noise performance

Converting an experiment to use a multiple point detector from a single point detector may pose some challenges. In the single point experiment, all of the light in the experiment is focused onto the detector and so there are unlikely to be issues with a lack of light power or spatial variation. In a multiple point detector, the beam profile of the illumination becomes important. If the beam is very tightly focused then only the pixels in the focus point will receive any light. If the beam is expanded so that the array is fairly uniformly illuminated then a large part of the beam will be wasted because it is not on the array. The programmable gain feature can help in this instance.

Consider the case where we have a signal where the modulated component that we want to measure is 10,000 times smaller than the background intensity and that we are using the full well setting on all pixels. At a pixel that is strongly illuminated and almost filling the well, each channel measurement will consist of approximately 600 Me$^-$. Assuming the dominant source of noise in the camera is shot noise, we have shot noise of 24.5 ke$^-$ and a signal to noise ratio (SNR) of 24,500. Now consider a pixel with only 20% of the illumination intensity. Each channel is receiving 120 Me$^-$ so has a shot noise limited SNR of 11,000. Both pixels can make the measurement in a single shot.

We have assumed the camera is dominated by shot noise. Other sources of noise in the camera are reset noise and read noise. Reset noise is the thermal noise present on the integration capacitance in the pixel during reset and is calculated as $\sqrt{kT/C}$ (volts), where k is Boltzmann's constant, T is temperature in Kelvin and C is the capacitance in Farads. With a full well setting of 35.3 pF, the reset noise for each channel is 10.8 µV at room temperature. We have performed simulations with the Cadence Spectre simulator to obtain the expected read noise at the pad of the chip. In a bandwidth of 2 MHz, the read noise is 41 µV. The noise sources are uncorrelated so they add in quadrature to give a total noise of 42.4 µV which is equivalent to 9.4 ke$^-$ with a full well setting. When this noise contribution is added to the shot noise the SNR for the bright pixel is 22,900 and 8300 for the dim pixel. The dim pixel can no longer meet the measurement requirement in a single shot.

The read noise for the camera should remain the same regardless of the gain setting. This means that using the gain settings to match the well size at each pixel to the light intensity falling on it will improve performance: the voltage signal at the output of the pixel will be amplified as much as possible. We are increasing the signal without increasing the noise. For the dim pixel with full well setting, the signal of interest of 60 ke$^-$ is equivalent to a change in voltage of 54 µV. At a gain setting of $n=2$ with a well depth of 124.9 Me$^-$ the same signal is equivalent to 259 µV. From a noise perspective, the shot noise remains the same because the number of photons absorbed is the same. The reset noise increases to 24 µV due to the reduced capacitance and the read noise remains the same at 41 µV, for a total of 47.5 µV or 2.2 ke$^-$. The total equivalent noise in electrons is 11.2 ke$^-$ which results in an SNR of 10,700.

3. EXPERIMENTAL NOISE RESULTS

3.1 Dark Noise

In this experiment, the camera is operated exactly as it would be in normal operation except the sensor is protected from light. This allows the read noise of camera to be evaluated without being influenced by noise in the light source or differing levels of illuminations at different pixels. The camera was operated using its internal modulation clock set to 1 kHz and data sets were taken for four different well settings, 11 capacitors (full well), 5 capacitors, 1 capacitor and 0 capacitors. Figure 5 shows the per-pixel noise for a single channel taken over 5000 frames. Although there is a noticeable difference in the noise values between pixels, the important point is that there is only a small variation in noise level between the different well levels. The mean variation in noise between the wells is 1.4 µV. The channel to channel variation shows a similar pattern with a mean variation of 2.3 µV.
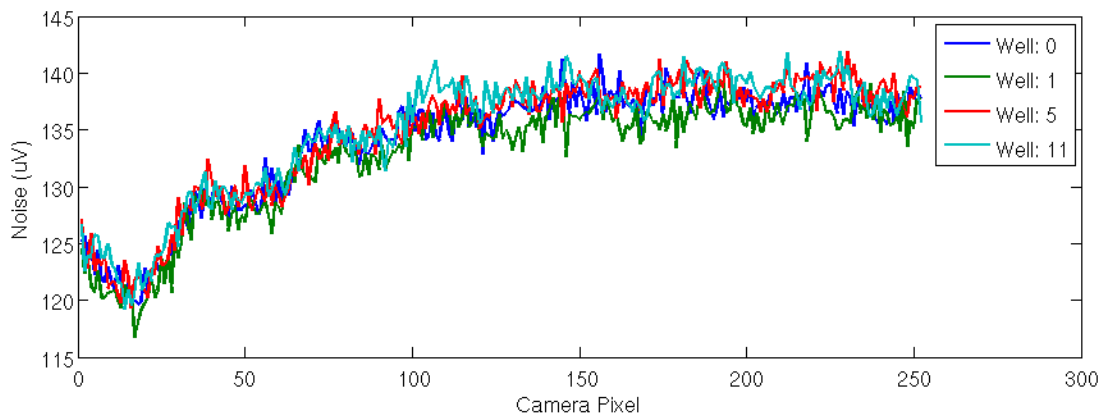

Figure 5. Dark noise across multiple well settings.

The peak noise level of around 140 µV is greater than predicted by the circuit simulation, but is accounted for by the external components used in the digitization process. At full well depth of this noise is equivalent to 31 ke⁻ shot noise which means that a demodulated image with greater than 950 Me⁻ total will be shot noise limited, or approximately 40% full on all channels. With a single capacitor connected, 140 µV is equivalent to 3.8 ke⁻ shot noise so 14 Me⁻ are needed to be shot noise limited, or approximately 19% on all channels.

3.2 D.C. Illuminated Noise

Figure 6 shows the equivalent result to Fig. 5 when the camera is illuminated with a light emitting diode, focused to be as uniform as possible on the sensor. The light intensity remained the same for each well setting. The overall noise level has increased due to the light source, but now it can be seen that the noise level is dependent on the well setting as would be expected if the noise is coming from the illumination.
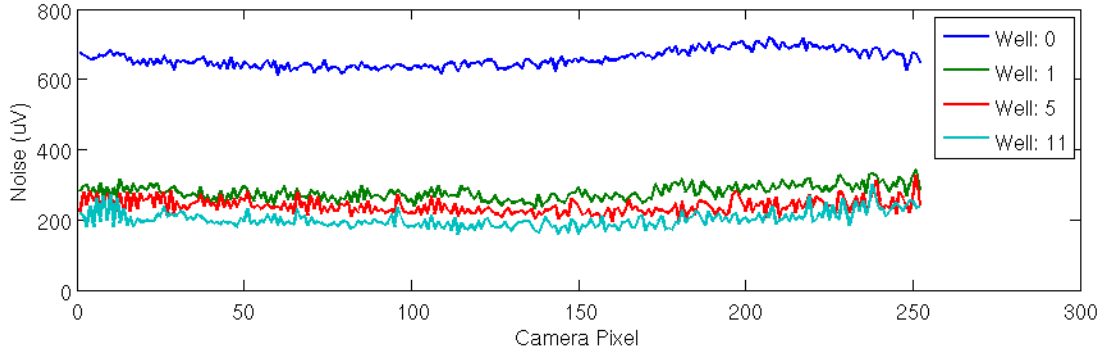

Figure 6. Noise under D.C. illumination.

4. OPTICAL SETUP

We have performed pump-probe picosecond ultrasound experiments[15] with our detector. The experimental setup is shown in Fig. 6. The output of a narrow width pulsed laser (spectra physics Tsunami, 100 fs pulse width, 80 MHz repetition rate, 800 nm wavelength) is split into two arms, the pump and the probe. The pump beam passes through a mechanical chopper controlled by the detector to provide the low frequency modulation signal. It is then focused to a ~3 µm spot onto the sample by a 0.6 NA objective lens. As the pulse from the pump beam is absorbed by the sample, there is rapid local heating the sample experiences thermal expansion. The thermal expansion produces an acoustic wave that propagates into the sample.

The probe beam passes along an optical delay line, is focused to the same point on the sample as the pump beam, is reflected from the sample and then onto a grating to disperse the spectrum and the first order is focused onto the array detector so each pixel measures a different probe wavelength. Changing the length of the delay line allows the time at which the probe beam arrives at the sample to be varied and so control which part of the acoustic wave is being interrogated.

The sample in this experiment is GaAs <111>, which is semi-transparent at the wavelengths in use. As the acoustic wave propagates into the sample, one part of the probe beam is reflected at the sample/air interface and another part is reflected at the acoustic wave. The two reflected components mix together in the form of an interferometer and because the acoustic wave is moving, the phase between the two components will oscillate. This type of signal is termed Brillouin oscillations[16].

The oscillation frequency is given by equation 9, where v_a is the acoustic velocity of the sample (~5400 m/s), n is the real part of the refractive index of the sample (~3.7), λ is the wavelength (~800-815 nm) of the probe beam and ϑ is the angle of incidence of the probe beam, which is zero in our case.

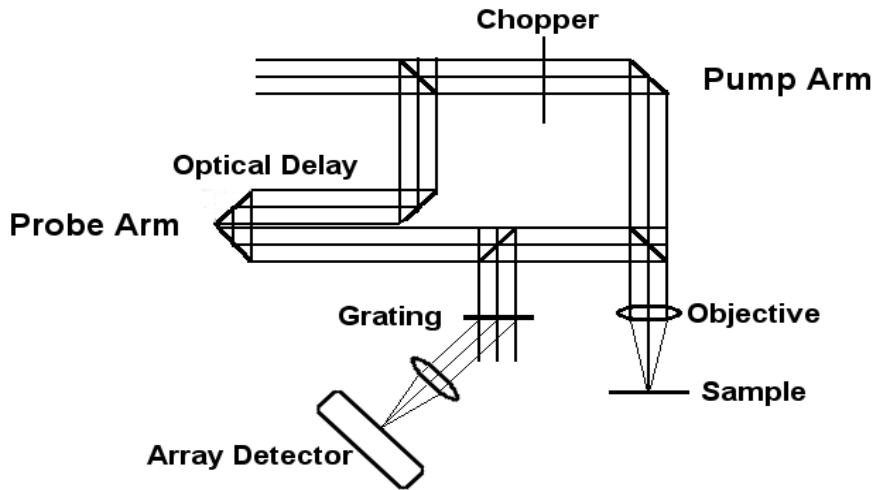$$f_b = \frac{2v_a n}{\lambda} \cos \vartheta \tag{9}$$

Figure 6. Pump-probe experiment optical arrangement

The small change in reflectivity on the order of 1 part in 10^5 or 10^6 which is caused by the acoustic wave can be detected by modulating the pump beam with a chopper so the reflectivity is switched between with and without the pump beam, or with and without the acoustic wave. This small fluctuation carries the information we are interested in about the acoustic wave. The grating is used to disperse the different probe beam wavelengths onto the detector, where each pixel measures a different oscillation frequency, as calculated from equation 9. By replacing the single point detector with our linear detector we are able to measure the interaction of the probe beam and different acoustic frequencies within the sample in a single parallel measurement.

5. RESULTS

This experiment was carried out with our old acquisition system which uses a National Instruments PCI-6281, an 18-bit 500 ksps acquisition card. The modulation frequency was set to 450 Hz. The light was dispersed across the detector with a 600 line/mm grating and focused onto the detector by a lens with focal length of 100 mm. Each pixel therefore corresponds to a change in probe wavelength of ~0.12 nm, for a total optical bandwidth across the detector of ~16 nm.

In this experiment, the laser was deliberately focused to a sharper point than would normally be used, in order to allow the use of the well settings to be demonstrated. Two sets of experiments were run, the first where all the well settings were set to the maximum and the second where the well settings were matched to the profile to give a better response.
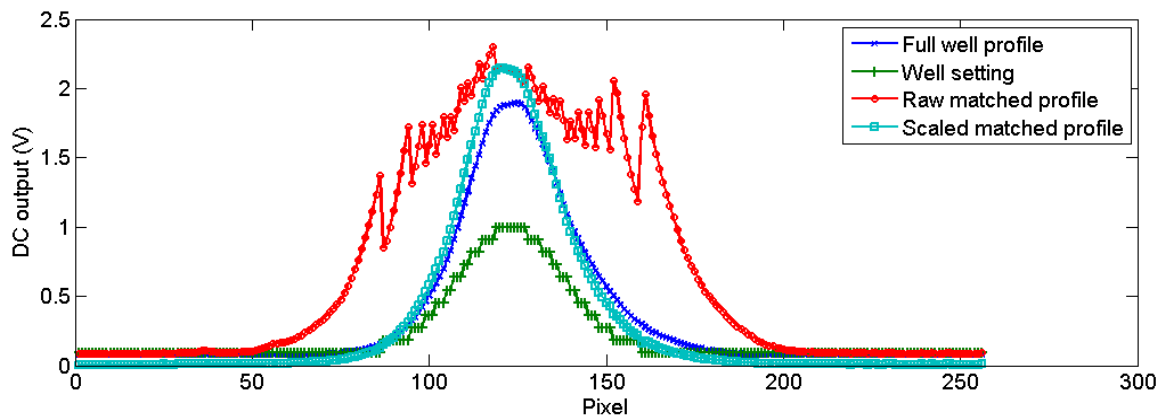

Figure 7. D.C. beam profile and well setting.

Figure 7 shows the profile for the full well setting, the raw profile retrieved when the matched well settings are applied and the scaled profile taking the well settings into account.

The signals obtained from this type of experiment usually have three main components, a step change in the response at time t=0 where the pump and probe beams are temporally aligned (coincident peak), a slow thermal relaxation curve and superimposed on this is the oscillating signal of interest. 200 averages were used in these experiments. Figure 8 shows the demodulated output from the detector after the thermal background was removed by subtracting a low order polynomial curve for both the raw data from both experiments on the left and the data after well depth scaling has been applied, on the right. The image with matched wells shows a much reduced noise content and a clearer signal. The measured oscillations are well defined and the signals are visible over the center detector pixels. The modulation depth of the recovered signals is ~0.5x10-4 → 1x10-5 with respect to the d.c. light level.
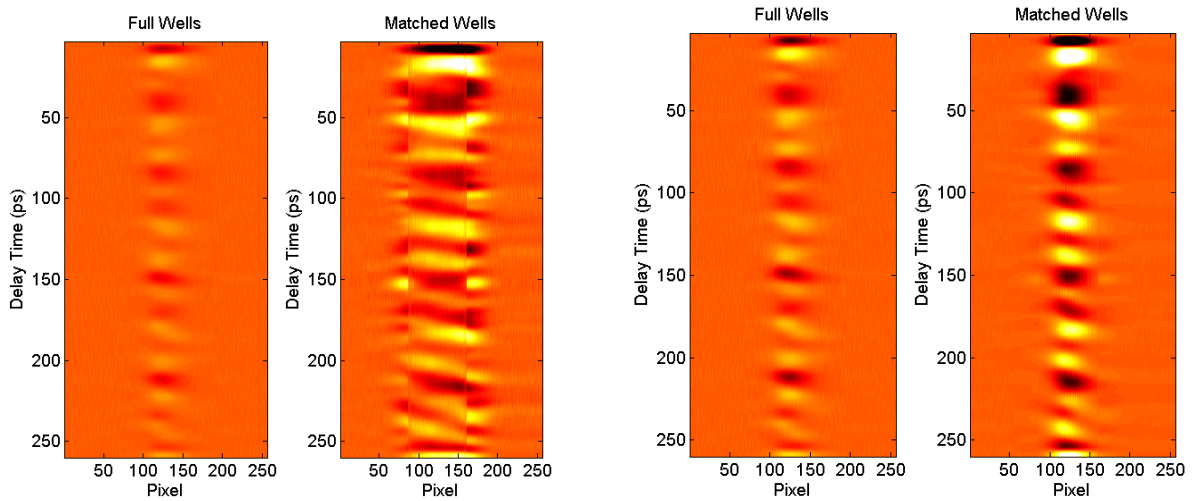

Figure 8. Recovered acoustic waves. Left: Raw data. Right: With well depth scaling applied.

Figure 9 shows the oscillation frequency recovered from the data shown in Fig. 8. The area outside the center of the detector does not have enough signal to recover the frequency accurately in both cases. The matched well case shows a more linear response than the full well case and also extends the region of useful signal as can be seen on the left hand side of the plot from approximately pixel 90-105, which is an increase of 1.2 nm in the wavelength that can be interrogated.
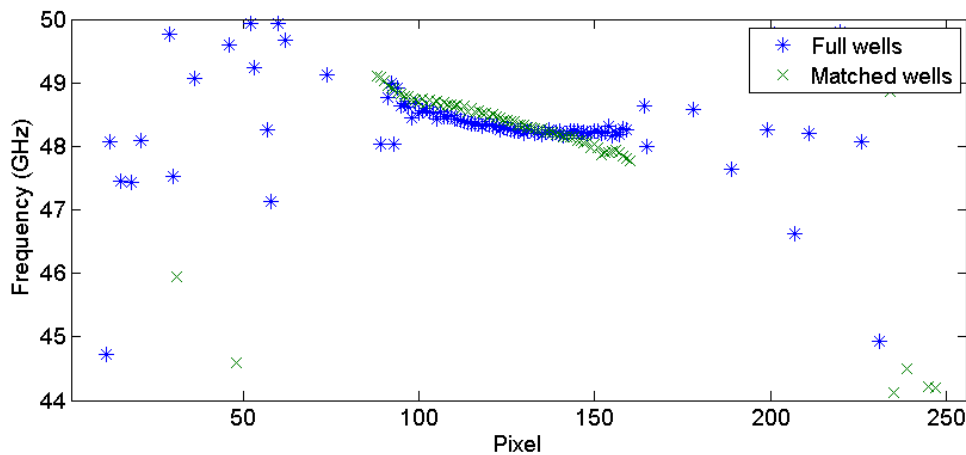

Figure 9. Calculated oscillation frequency for full and matched well results

6. CONCLUSIONS

A 256 pixel linear sensor has been presented. Each pixel has four independent very large wells, making the detection of modulated signals in the presence of high background illumination possible. The capability of detecting signals of the order of 10^{-5} of the background illumination level has been demonstrated. The sensor is usable over a range of illuminations and can be tailored to provide the best voltage response to a specific illumination profile through the use of the per-pixel variable gain. The variable gain also extends the range over which the sensor is shot noise limited, from 60% of the effective well depth if only the largest well were available to 81% of the effective well depth when operating at a sampling frequency of 1.9 MHz.

REFERENCES

1. Boulade, O., Charlot, X., Abbon, P., Aune, S., Borgeaud, P., Carton, P., Carty, M., Da Costa, J., Deschamps, H., et al., "MegaCam: the new Canada-France-Hawaii Telescope wide-field imaging camera," in Instrument Design and Performance for Optical/Infrared Ground-based Telescopes 4841, 72-81 (2003).
2. Holland, S., Bebek, C., Daniels, P., Dawson, K., Ernes, J., Groom, D., Jelinksy, S., Karcher, A., Kolbe, W., et al., "Technology development for 4k × 4k, back-illuminated, fully depleted scientific CCD imagers," in Nuclear Science Symposium Conference Record 2007 2220-2225 (2007).
3. Yadid-Pecht, O., and Fossum, E., "Wide intrascene dynamic range CMOS APS using dual sampling," IEEE Transactions on Electron Devices 44(10), 1721-1723 (1997).
4. Hosticka, B., Brockherde, W., Bussmann, A., Heimann, T., Jeremias, R., Kemna, A., Nitta, C., and Schrey, O., "CMOS imaging for automotive applications," IEEE Transactions on Electron Devices 50(1), 173-183 (2003).
5. Ide, N., Lee, W., Akahane, N., and Sugawa, S., "A Wide DR and Linear Response CMOS Image Sensor with Three Photocurrent Integrations in Photodiodes, Lateral Overflow Capacitors, and Column Capacitors," IEEE Journal of Solid-State Circuits 43(7), 1577-1587 (2008).
6. Cheng, H., Choubey, B., and Collins, S., "An Integrating Wide Dynamic-Range Image Sensor with a Logarithmic Response," IEEE Transactions on Electron Devices 56(11), 2423-2428 (2009).
7. Guo, J., and Sonkusale, S., "An auto-switched mode CMOS image sensor for high dynamic range scientific imaging applications," in IEEE Sensors 2008, 355-358 (2008).
8. Smith, R.J., Light, R.A., Sharples, S.D., Johnston, N.S., Pitter, M.C and Somekh, M.G., "Multichannel, time-resolved picosecond laser ultrasound imaging and spectroscopy with custom complementary metal-oxide-semiconductor detector," Review of Scientific Instruments 81(2), 024901-6 (2010).
9. Spirig, T., Seitz, P., Vietze, O., and Heitger, F., "The lock-in CCD-two-dimensional synchronous detection of light," IEEE Journal of Quantum Electronics 31(9), 1705-1708 (1995).
10. Oike, Y., Ikeda, M., and Asada, K., "High-performance photo detector for correlative feeble lighting using pixel-parallel sensing," IEEE Sensors Journal 3(5), 640-645 (2003).
11. Bourquin, S., Seitz, P., and Salathe, R., "Two-dimensional smart detector array for interferometric applications," Electronics Letters 37(15), 975-976 (2001).
12. Ando, S., and Kimachi, A., "Correlation image sensor: two-dimensional matched detection of amplitude-modulated light," IEEE Transactions on Electron Devices 50(10), 2059-2066 (2003).
13. Pitter, M., Light, R., Somekh, M., Clark, M., and Hayes-Gill, B., "Dual-phase synchronous light detection with 64×64 CMOS modulated light camera," Electronics Letters 40(22), 1404-1405 (2004).
14. Johnston, N., Stewart, C., Light, R., Hayes-Gill, B., Somekh, M., Morgan, S., Sambles, J., and Pitter, M., "Quad-phase synchronous light detection with 64 X 64 CMOS modulated light camera," Electronics Letters 45(21), 1090-1091 (2009).
15. Wright, O.B., Hyoguchi, T., and Kawashima, K., "Laser Picosecond Acoustics in Thin Films: Effect of Elastic Boundary Conditions on Pulse Generation," Japanese Journal of Applied Physics 30, L131-L133 (1991).
16. Thomsen, C., Grahn, H., Maris, H., and Tauc, J., "Picosecond interferometric technique for study of phonons in the Brillouin frequency range," Optics Communications 60(1-2), 55-58 (1986).